ELSEVIER

Thin Solid Films 384 (2001) 76–84

thin solid films

www.elsevier.com/locate/tsf

# Fluorescent apparent quantum yields for excited molecules near dielectric interfaces

Q.Q. Shu*,[a], P.K. Hansma[b]

[a] *Department of Materials Science and Engineering, School of Science, Shenzhen University, Shenzhen, Guangdong 518060, PR China*
[b] *Department of Physics, University of California, Santa Barbara, CA 93106, USA*

Received 1 March 2000; received in revised form 21 August 2000; accepted 12 October 2000

**Abstract**

Fluorescence energy transfer from excited molecules to dielectric medium interfaces was modeled as a many-dipole system. A formula for the apparent quantum yield $q_a$, which expresses the ratio of the energy flux above the emitting dipoles to the total power emitted by these dipoles, was derived. The distances between $Eu^{3+}$ ions of europium(III) thenoyltrifluoroacetonate (EuTTA) and the dielectric interfaces were controlled with alumina spacers of varied thickness, and the distance-dependence of the fluorescence intensity of the $Eu^{3+}$ ions was measured. The $q_a$ for 25 dielectric systems, where the emitting centers are located in alumina at a distance of 20 Å from the interfaces, was calculated. Comparison between the calculated and experimental $q_a$ shows that the fluorescence energy transfer can be explained by the classical electromagnetic theory. At the short distance (10–50 Å), the fluorescence quenching is very strong for almost all materials. For example, the emitting centers within 20 Å of a transparent conductor $In_2O_3$ film surface will be quenched to below 1% of its normal fluorescence. Thus, the calculated $q_a$ may be considered as a characteristic parameter to evaluate materials for possible inclusion in diverse light-emitting devices. 

*Keywords:* Dielectrics; Fluorescence; Interfaces; Energy transfer

## 1. Introduction

Distance-dependent fluorescent energy transfer from excited molecules to a dielectric surface or acceptor molecules has been widely investigated by observing the fluorescent lifetime and intensity [1–5]. For example, the energy transfer from $^3n\pi^*$ pyrazine to GaAs(110) was studied by measuring the distance-dependence of its lifetime [3]; fluorescence resonance energy transfer between dye molecules over a range of 10–100 Å was studied by using a scanning near-field optical microscope or atomic force microscope [4]; and distance-dependent energy transfer between indole and anthracene moieties in Langmuir–Blodgett films was studied by measuring fluorescent spectra, where the monolayers of the donor and acceptor can be precisely separated by inert spacers of stearic acid layers of varied thickness [5]. What we are interested in is how, due to the non-radiative energy transfer from excited molecules to dielectric interfaces at short distances (10–50 Å), the fluorescence intensity changes as the distance varies. In this paper, following the energy flux method, we modeled an assembly of the excited molecules as a many-dipole system and derived a formula for a measurable quantity, i.e., apparent quantum yield $q_a$, and then made the comparison of the calculated $q_a$ with the observed distance-dependent fluorescent intensity of $Eu^{3+}$ ions of europium(III) thenoyltrifluoroacetonate (EuTTA) near dielectric interfaces, where the separation between the $Eu^{3+}$ ions

* Corresponding author.
*E-mail address:* shuqq@szu.edu.cn (Q.Q. Shu).

0040-6090/01/$ - see front matter 
PII: S0040-6090(00)01809-5

and dielectric interfaces is precisely controlled by non-absorbing alumina films of different thickness.

## 2. Theory

In the classical electromagnetic description of the fluorescent energy transfer from an excited molecule to a dielectric interface between two media, the emitting molecule is treated as an oscillating dipole. The geometry of the problem is shown in Fig. 1. The two regions are half spaces, with dielectric constants given as $\varepsilon_j = n_j^2 - k_j^2 + i2n_jk_j$, where $n_j$ and $k_j$ ($j = 1,2$) are the real and imaginary parts of the refractive indices of regions 1 and 2, respectively. Following the energy flux method of single dipole [6], the fluxes $F_{\uparrow}^{\perp}$ and $F_{\downarrow}^{\perp}$, contained in the regions above and below a perpendicular dipole, respectively, located at distance from the dielectric interface, are given by:

$$F_{\uparrow}^{\perp} = \left[\frac{E_0}{\tau_0}\right] q \left[1 - \tfrac{3}{4}\mathrm{Im}\int_0^1 [1 - |R^{\parallel}|^2]\frac{u^3}{l_1}\mathrm{d}u - \tfrac{3}{2}\mathrm{Im}\int_0^1 R^{\parallel} e^{-2l_1\hat{d}}\frac{u^3}{l_1}\mathrm{d}u\right] \quad (1)$$

$$F_{\downarrow}^{\perp} = \left[\frac{E_0}{\tau_0}\right] q \left[\tfrac{3}{4}\mathrm{Im}\int_0^1 [1 - |R^{\parallel}|^2]\frac{u^3}{l_1}\mathrm{d}u - \tfrac{3}{2}\mathrm{Im}\int_1^{\infty} R^{\parallel} e^{-2l_1\hat{d}}\frac{u^3}{l_1}\mathrm{d}u\right] \quad (2)$$

where $E_0 = (1/2)m\omega^2|\vec{\mu}|^2/e^2$ ($e$ is the charge and $m$ is the effective mass of the dipole of moment $\vec{\mu}$ and frequency of oscillation $\omega$) is the total energy of the single dipole; $\tau_0$ is lifetime of the dipole in the absence of the interface; $q$ is quantum yield of free emitting dipole without the dielectric interface; $\hat{d} = k_1 d$, $k_1 = n_1\omega/c$, $c$ is the speed of light; $R^{\parallel}$ is the reflection coefficient for an incident ray polarized parallel to the incidence plane ($p$-polarized):

$$R^{\parallel} = \frac{\varepsilon_1 l_2 - \varepsilon_2 l_1}{\varepsilon_1 l_2 + \varepsilon_2 l_1} \quad (3)$$

and

$$l_1 \equiv -i(1-u^2)^{1/2} \text{ and } l_2 \equiv -i(\varepsilon_2/\varepsilon_1 - u^2)^{1/2} \quad (4)$$

The total power absorbed by the dipole is:

$$F_{\text{total}}^{\perp} = F_{\uparrow}^{\perp} + F_{\downarrow}^{\perp} + F_{\text{nr}} \quad (5)$$

where $F_{\text{nr}} = (E_0/\tau_0)(1-q)$ is the rate of the intrinsic non-radiative power loss by the dipole without the dielectric interface. Eq. (5) is valid for parallel dipoles,

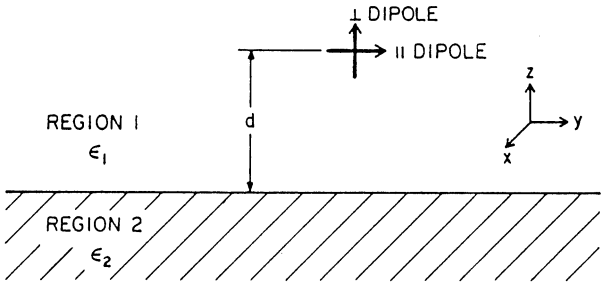


Fig. 1. Geometry for an emitting molecule acting as an oscillating dipole near a dielectric interface between two semi-infinite media of the dielectric constants $\varepsilon_1$ and $\varepsilon_2$.

except that $F_{\uparrow}^{\perp}$ and $F_{\downarrow}^{\perp}$ are replaced by those for parallel dipoles, $F_{\uparrow}^{\parallel}$ and $F_{\downarrow}^{\parallel}$:

$$F_{\uparrow}^{\parallel} = \left[\frac{E_0}{\tau_0}\right] q \left[1 - \tfrac{3}{8}\mathrm{Im}\int_0^1 [(1 - |R^{\perp}|^2) + (1-u^2) \times (1 - |R^{\parallel}|^2)]\frac{u}{l_1}\mathrm{d}u + \tfrac{3}{4}\mathrm{Im}\int_0^1 \times [R^{\perp} + (1-u^2)R^{\parallel}]e^{-2l_1\hat{d}}\frac{u}{l_1}\mathrm{d}u\right] \quad (6)$$

$$F_{\downarrow}^{\parallel} = \left[\frac{E_0}{\tau_0}\right] q \left[\tfrac{3}{8}\mathrm{Im}\int_0^1 [(1 - |R^{\perp}|^2) + (1-u^2) \times (1 - |R^{\parallel}|^2)]\frac{u}{l_1}\mathrm{d}u + \tfrac{3}{4}\mathrm{Im}\int_1^{\infty} \times [R^{\perp} + (1-u^2)R^{\parallel}]e^{-2l_1\hat{d}}\frac{u}{l_1}\mathrm{d}u\right] \quad (7)$$

where $R^{\perp}$ is the reflection coefficient for the incident ray polarized perpendicular to the incidence plane ($s$-polarized):

$$R^{\perp} = \frac{l_1 - l_2}{l_1 + l_2} \quad (8)$$

The physical implication of the reflection coefficients $R^{\parallel}$ and $R^{\perp}$ can be stated as follows: in the energy flux Eqs. (1)–(4), the first integral expression is, in each case, related to the interface absorption effect on the photons directly emitted by the dipole. They are equal to zero for a perfect interface ($R^{\parallel} = R^{\perp} = -1$) and equal to $(E_0/\tau_0)/2$ for a non-reflective interface ($R^{\parallel} = R^{\perp} = 0$), i.e. there is no boundary.

As can be seen in Eq. (1), the energy flux above the dipole consists of three parts: (i) the first term is the total power emitted by the dipole in the absence of the dielectric interface, $(E_0/\tau_0)q$; (ii) the second term is power loss due to the absorption of photons at the interface, the sign of term is always negative; and (iii) the third term is the power redirected to the region above the dipole by the reflection of photons at the

interface, and it results in wide-angle interference, since it contains the phase factor dependent on the distance $d$ [7]. As stated above, if there is no boundary, the sum of the three terms is $(E_0/\tau_0)/2$.

As shown in Eqs. (2) and (7), the power below the dipole flows to the interface in two ways: one, described previously, is the absorption of photons at the interface, which is associated with the far field of the dipole; another is the non-radiative energy transfer to the interface, which is represented by an integral in the interval $1 \rightarrow \infty$ with a factor $e^{-2l_1\hat{d}}$. Because $l_1$ is real for $1 < u < \infty$, the factor $e^{-2l_1\hat{d}}$ is a real exponential decay factor with distance $d$. According to the classical electromagnetic theory, the near field of the dipole is the static electric field in nature and varies as the minus third power of the distance from the dipole. Therefore, the non-radiative energy transfer has its origin in the near field of the dipole and occurs over a small distance range of 10–50 Å from the interface.

Fig. 2 shows plots of the computed power absorbed by the dipole and the power emitted by the dipole embedded in a semi-infinite alumina versus the distance of the dipole from the dielectric interface, for both perpendicular and parallel dipoles. The power flow below the dipole is not directly shown in these figures because: (i) in the small distance range it is almost the same as the total power flow absorbed by the dipole; and (ii) it decreases very quickly as the distance from the interface increases, and is negligible at large distances. Note that, due to the exponential decay of the non-radiative energy with the distance and the interference at the large distances, both the total absorbed power and the energy flux above the dipole oscillate with the distance. However, as can be seen in Fig. 2, at short distances, the energy transfer to the interface increases drastically and not at the expense of a remarkable decrease in the energy flux above the single dipole. In fact, what we would like to do is to determine the energy transfer from many excited molecules (not from a single excited molecule) to the dielectric interface by measuring the energy flux above the interface. Experimentally, for a practical system consisting of a dielectric interface and many excited molecules close to it, the measured energy flux above the interface is strongly dependent on the distances of the excited molecules from the interface. In particular, at short distances the measured energy flux above the interface decreases drastically as the distance decreases. This suggests that, for a practical system consisting of a dielectric interface and many excited molecules close to it, the number of the excited (emitting) molecules (dipoles) in unit time increases drastically as the distance ($< 50$ Å) between the interface and molecules decreases. Therefore, for a many-dipole (many excited molecules) system, in which each dipole is located at the same distance $d$ from the interface, if $N^{\perp}(d)$ is the number of perpendicular emitting dipoles in the unit, the total energy flux above the many-dipole system, due to these perpendicular emitting dipoles, can be written as follows:

$$\Phi_{\uparrow}^{\perp} = N^{\perp} F_{\uparrow}^{\perp} \tag{9}$$

where $F_{\uparrow}^{\perp}$ is the energy flux above a single perpendicular dipole and is given by Eq. (1). Introducing the incident power $I_0^{\perp}$ responsible for exciting perpendicular dipoles, $N^{\perp}$ can be obtained from:

$$N^{\perp} = I_0^{\perp}/F_{\text{total}}^{\perp} \tag{10}$$

where $F_{\text{total}}^{\perp}$ is the total power absorbed by a single perpendicular dipole and is given by Eq. (5). Substituting Eq. (10) into Eq. (9), we obtain the total energy flux above the perpendicular dipoles for the many dipole system:

$$\Phi_{\uparrow}^{\perp} = I_0^{\perp} F_{\uparrow}^{\perp}/F_{\text{total}}^{\perp} = I_0^{\perp} q_{\text{a}}^{\perp} \tag{11}$$

where $q_a^{\perp} \equiv F_{\uparrow}^{\perp}/F_{\text{total}}^{\perp}$ is the apparent quantum yield of a single perpendicular dipole, defined as the ratio of the energy flux above the emitting dipole to the total power emitted by this dipole. Note that the apparent quantum yield must be distinguished from the quantum yield of the emitting state; the latter is the probability that a molecule in the excited state will emit a quantum of fluorescent light.

Similarly, the total energy flux above the parallel dipoles for this many dipole system, $\Phi_{\uparrow}^{\parallel}$, can be obtained as follows:

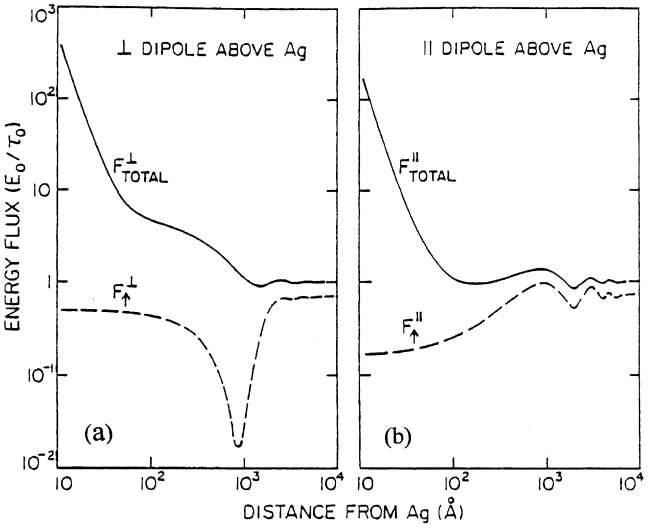


Fig. 2. The calculated total power emitted by a dipole located in a semi-infinite alumina ($\varepsilon_1 = 2.89 + i0$) and energy flux above the dipole versus the distance from the surface of Ag ($\varepsilon_2 = -15.36 + i0.23$). The emission wavelength and quantum yield of the free emitting state ($q$) is taken to be 6120 Å and 0.70, respectively.

$$\Phi_{\uparrow}^{\parallel} = N^{\parallel} F_{\uparrow}^{\parallel} \tag{12}$$

$$N^{\parallel} = I_0^{\parallel} / F_{\text{total}}^{\parallel} \tag{13}$$

$$\Phi_{\uparrow}^{\parallel} = I_0^{\parallel} F_{\uparrow}^{\parallel} / F_{\text{total}}^{\parallel} = I_0^{\parallel} q_{\text{a}}^{\parallel} \tag{14}$$

$$F_{\text{total}}^{\parallel} = F_{\uparrow}^{\parallel} + F_{\downarrow}^{\parallel} + F_{\text{nr}} \tag{15}$$

where $N^{\parallel} = N^{\parallel}(d)$ is the number of the parallel emitting dipoles in unit time; $I_0^{\parallel}$ is the exciting power for the parallel dipoles; $F_{\uparrow}^{\parallel}$ and $F_{\downarrow}^{\parallel}$ are given by Eqs. (6) and (7), respectively; $F_{\text{nr}}$ is the same as that in Eq. (5); $q_{\text{a}}^{\parallel}$ is the apparent quantum yield of a single parallel dipole.

In order to determine $I_0^{\perp}$ and $I_0^{\parallel}$, consider a dipole of moment $\vec{\mu}$ and oriented at an angle $\theta$ relative to the normal to the interface. The dipole moment can be resolved into its perpendicular and parallel components: $|\vec{\mu}|\cos\theta$ and $|\vec{\mu}|\sin\theta$. Since the total power emitted by a dipole is proportional to the square of the magnitude of the dipole moment, the total power emitted by this oblique dipole is $|\vec{\mu}|^2(A^{\perp}\cos^2\theta + A^{\parallel}\sin^2\theta)$, where $A^{\perp}$ and $A^{\parallel}$ are proportionality constants. For a many-dipole system, the distribution of the dipole orientation can be taken to be random (isotropic), so that the expected total power emitted is given by taking the following average:

$$\frac{1}{2\pi}\int_0^{2\pi} d\phi \int_0^{\pi} d\theta |\vec{\mu}|^2 (A^{\perp}\cos^2\theta + A^{\parallel}\sin^2\theta) = |\vec{\mu}|^2 (\tfrac{1}{3}A^{\perp} + \tfrac{2}{3}A^{\parallel}) \tag{16}$$

This means that, for a many-dipole system with a random distribution of dipole orientation, the total power emitted by each dipole is the arithmetic average of the total power emitted by one perpendicular component and two parallel components. According to energy conservation, the total exciting power is equal to the total emitted power plus the power lost due to the intrinsic non-radiative channels. Thus, the total exciting power for the parallel dipoles is two-fold larger than that for the perpendicular dipoles:

$$\frac{I_0^{\perp}}{I_0^{\parallel}} = \frac{1}{2} \tag{17}$$

because both the perpendicular and parallel dipoles have the same rate of the intrinsic non-radiative power loss.

Finally, for a many-dipole system with the random distribution of dipole orientation, the total energy flux above the dipole, $\Phi_{\uparrow}$, can be written as:

$$\Phi_{\uparrow} = \Phi_{\uparrow}^{\perp} + \Phi_{\uparrow}^{\parallel} = I_{\uparrow}^{\perp} q_{\text{a}}^{\perp} + I_{\uparrow}^{\parallel} q_{\text{a}}^{\parallel} \tag{18}$$

where $\Phi_{\uparrow}^{\perp}$ and $\Phi_{\uparrow}^{\parallel}$ are given by Eqs. (11) and (14), respectively. Using Eq. (17), the above expression can be rewritten as:

$$\Phi_{\uparrow} = I_0^{\perp}(q_{\text{a}}^{\perp} + q_{\text{a}}^{\parallel}) = I_0 q_{\text{a}} \tag{19}$$

where $I_0 = 3I_0^{\perp}$ is the total incident power, an exciting power parameter determined by the experimental arrangement; and:

$$q_{\text{a}} = (1/3)(q_{\text{a}}^{\perp} + 2q_{\text{a}}^{\parallel}) \tag{20}$$

is the apparent quantum yield of the many dipole system with the random distribution of dipole orientation. It expresses the ratio of the energy flux above the emitting dipoles to the total power emitted by these dipoles. Note that $q_{\text{a}}$ can be determined by measuring the emission intensity integrated over the half space the emitting dipoles.

## 3. Experiment

The experimental detail has been given elsewhere [8,9]. As shown in the inset of Fig. 4a, the samples, prepared in a vacuum chamber, consist of an alumina spacer sandwiched between the top EuTTA sub-monolayer and one of the following the bottom dielectric films: metal (Ag), semiconductor ($In_2O_3$, $SnO_2$) and insulator ($Al_2O_3$). The slide holder, mask holder, shutters and different evaporation sources were combined and used alternately, so that 15 samples with different alumina spacer thickness could be prepared in situ on three microscope slides. Caution should be taken to control the thickness of EuTTA sub-monolayer. As the surface coverage of EuTTA molecules is less than a monolayer, this means that the interaction between $Eu^{3+}$ ions is not important. The distance between the $Eu^{3+}$ ions and the dielectric surfaces can be controlled by depositing the alumina spacers with different thickness. The fluorescent light (6120 Å) of EuTTA molecules illuminated by UV light (3650 Å) was collected by a scanning monochromator. By means of a photomultiplier, picoammeter and strip-chart recorder, the fluorescence spectra of EuTTA molecules were obtained.

We measured the fluorescent intensity of $Eu^{3+}$ ions on alumina ($Al_2O_3$) and $In_2O_3$ films of varied thickness. It was found that fluorescent intensity for both alumina and $In_2O_3$ was almost independent of their film thickness, and that the fluorescent intensity of $Eu^{3+}$ ions on the alumina films is approximately a factor of 100 greater than that on the $In_2O_3$ films. Since the alumina films of varied thickness do not quench the fluorescence, they can be used as the

Table 1
The experimental complex refractive indices ($n + ik$) and dielectric constants ($\varepsilon_1 + i\varepsilon_2$) for Ag, $In_2O_3$ and $SnO_2$ films[a]

| | Complex refractive indices, $n_2 + ik_2$ | | Dielectric constant, $\varepsilon_{21} + i\varepsilon_{22}$ | |
|---|---|---|---|---|
| | 6328 Å (1.96 eV) | 3650 Å (3.40 eV) | 6328 Å (1.96 eV) | 3650 Å (3.40 eV) |
| Silver (Ag) | $0.0295 + i3.92$ | $0.0860 + i3.71$ | $-15.36 + i0.231$ | $-13.76 + i0.638$ |
| Tin(IV) oxide ($SnO_2$) | $2.14 + i1.97$ | $1.99 + i2.09$ | $0.699 + i8.43$ | $-0.408 + i8.32$ |
| Indium oxide ($In_2O_3$) | $2.30 + i0.0270$ | $3.40 + i0.0109$ | $5.29 + i0.124$ | $11.56 + i0.741$ |

[a] The dielectric constants were calculated with $\varepsilon_1 = n^2 - k^2$ and $\varepsilon_2 = 2nk$.

spacers between the EuTTA sub-monolayer and the dielectric media studied.

Complex refractive indices of Ag and $SnO_2$ films were measured with a null ellipsometer (Rudolph Research). The complex refractive indices of absorbing transparent films, $In_2O_3$, were determined by measuring the reflection and transmission, and a correction for the observed reflection and transmission at the back surface of the actual substrate was made. The experimental results are given in Table 1.

## 4. Results and discussion

Fig. 3 shows the comparison between the theoretical and experimental apparent quantum yield $q_a$ for $Eu^{3+}$ ions near the surfaces of for alumina ($Al_2O_3$). In this work, the exciting power parameter $I_0$ has been chosen so that the experiments can best fit the theory. By changing this parameter we can uniformly shift all the experimental points up or down. As can be seen in Fig. 3, the experiment agrees with the theory. This can be understood on the basis of the fact that, in the range of visible light, the glass slide is non-absorbing and transparent.

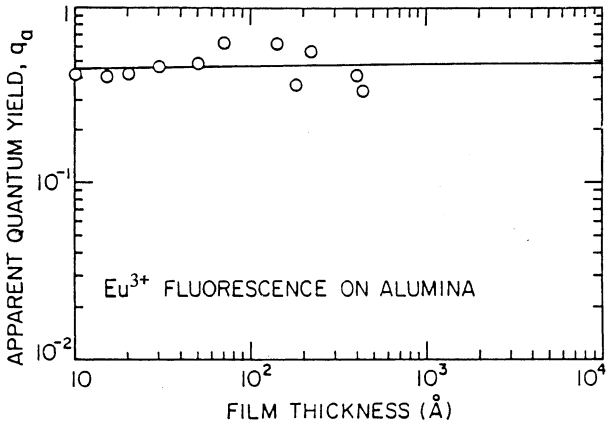


Fig. 3. Apparent quantum yield $q_a$ (experimental, open circles; and theoretical, solid curve) for $Eu^{3+}$ ions on alumina deposited on the microscope slide ($\varepsilon_2 = 2.46 + i0$). The quantum yield of the free emitting state ($q$) is taken to be 0.70. Note that both the theory and experiment show that alumina does not apparently quench fluorescence.

Fig. 4 shows the comparison between the theoretical and experimental apparent quantum yield $q_a$ for $Eu^{3+}$ ions near the surfaces of Ag, $SnO_2$ and $In_2O_3$, respectively. We can see that: (1) in the alumina spacer thickness range 10–50 Å, due to the non-radiative energy transfer from the $Eu^{3+}$ ions to the dielectric interfaces of Ag, $SnO_2$ and $In_2O_3$, the apparent quantum yield increases (quenching decreases) as the alumina spacer thickness (distance of the dielectric) increases, but the experimental data fall less rapidly than the theoretical curves with decreasing spacer thickness; and (2) due to the multiple-beam destructive interference between the incident and reflected exciting UV light at the interfaces, in the alumina spacer thickness range 600–800 Å, the experimental data show a dip. The multiple reflection of the plane waves at the different interfaces produces the multiple-beam interference, which is dependent on the dielectric properties of the interfaces, for example, on the reflection coefficients. Thus, the dip position differs in Ag, $SnO_2$ and $In_2O_3$ dielectrics. However, our calculated results show that in the alumina spacer thickness range 10–50 Å, the increases (or decreases) in the excitation intensity of the UV light are quite small, and not important. At a distance of 10–50 Å from the dielectric interfaces, the parameter of interest is the non-radiative energy transfer. On the other hand, as seen in Fig. 4, in the spacer thickness range 10–50 Å, each theoretical curve, without correction for the excitation intensity, falls more rapidly than the experimental data. It follows that the discrepancy between the experiment and theory, occurring in the spacer thickness range 10–50 Å, cannot be explained by introducing a correction for the excitation intensity into the theoretical treatment, because in this case the predominant effect is the non-radiative energy transfer.

The experimental data, which fall less rapidly than the theory with alumina spacers of 10–50 Å, could be explained by taking the surface roughness into account. First, the roughness in the dielectric interfaces tends to enhance the total emission intensity, due to the interaction between the excited molecules and the localized surface plasma resonances, whose resonant frequencies are sensitive functions of the shapes and sizes of the

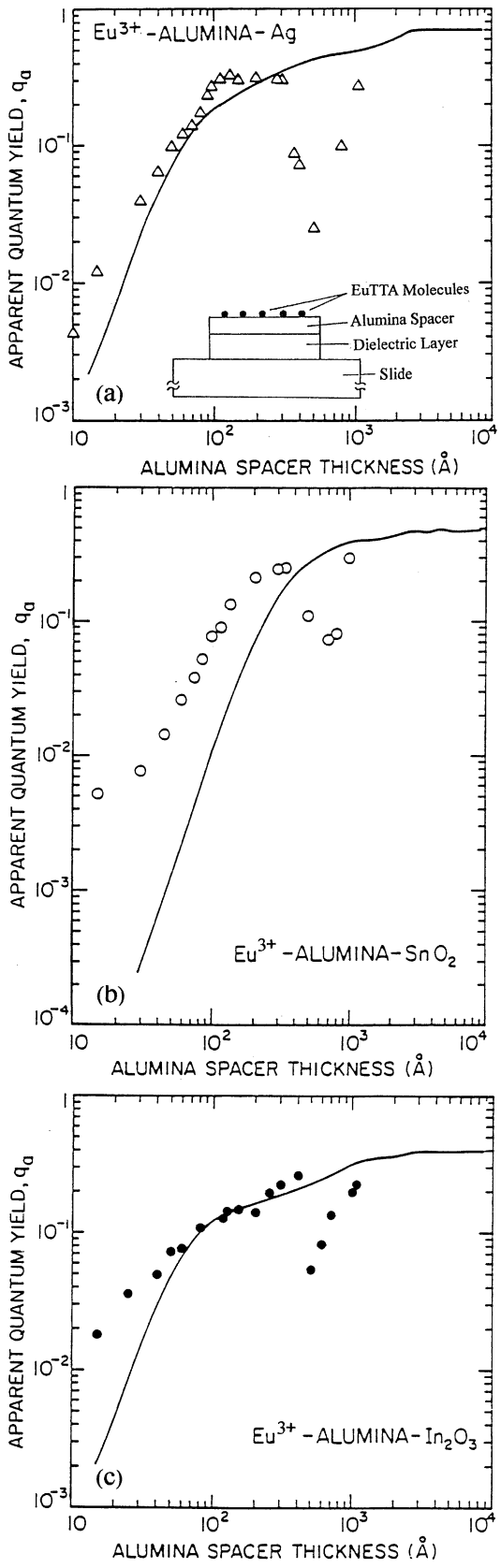


Fig. 4. Apparent quantum yield $q_a$ (experimental, open triangles, circles and closed circles; and theoretical, solid curve) for $Eu^{3+}$ ions which are separated from: (a) Ag;(b) $SnO_2$; and (c) $In_2O_3$ by alumina spacers. The quantum yield of the free emitting state ($q$) is taken to be 0.70. The inset in (a) shows a schematic of the sample structure.

roughness features on the surface [10]. If the UV light frequency is such that it can excite a surface plasma resonance, the dipoles induced at the rough surface will result in a large increase in the local field at the molecules, and lead to an increased absorption rate of the UV light. Similarly, the emitting dipole of a fluorescing molecule will be damped considerably at the emission frequency, due to the induced plasma resonances at the rough surface. The net increase in the total emission intensity results from a balance between the increase in the local field at the UV light frequency (i.e. pump frequency) and the increase in the non-radiative energy transfer to the surface at the emission frequency. Experimentally, such a net increase in the emission intensity has been observed [11]. Ag and $SnO_2$ can support these resonances because their dielectric constants have negative real parts. Thus, the observed apparent quantum yield for Ag and $SnO_2$ is larger than those predicted by the theory at a small spacer thickness.

Second, roughness in the alumina spacer can average the experimental data over the spacer thickness and make them decrease less rapidly, especially at a small spacer thickness. For example, a re-examination of the theoretical curve in Fig. 4c shows that if the alumina spacer consists of 50% regions 10 Å thick and 50% regions 20 Å thick, the apparent quantum yield obtained from the curve would be approximately $[(1+6)/2=]\ 3.5\times10^{-3}$, rather than $\approx 2.5\times10^{-3}$ for a 15 Å thick region on average. Clearly, a detailed knowledge of the roughness would be necessary to carry out quantitative modeling, but trend is clear: the roughness will decrease the slope of the theoretical curves in Fig. 4. This explanation can be used for the case of $In_2O_3$, since its surface does not support the surface resonances. On the other hand, our experimental data for $In_2O_3$ is in agreement with those for GaAs(110) obtained by Whitmore et al. [3] They measured the fluorescent lifetime as the function of the emitter-GaAs(110) surface separation and found that, at a short separation (< 100 Å), the observed lifetime decreases more rapidly than the theory predictions. Note that the lifetime is inversely proportional to the emission intensity. Thus, as far as the emission intensity is concerned, the experimental data will decrease less rapidly than the theory.

Table 2 shows the calculated apparent quantum yields, $q_a$, which is given by Eq. (20), for 25 dielectric systems ($\varepsilon_2=\varepsilon_{21}+i\varepsilon_{22}$), where emitting centers are located in alumina ($\varepsilon_1=\varepsilon_{11}+i\varepsilon_{12}=2.89+i0$) at a distance of 20 Å from the surfaces of the dielectric media. Of 25 dielectrics, almost all materials have important applications in industrial production and scientific research: Au, Ag, Pt and Ir are noble metals; Si and Ge are the semiconductors most in use; $Al_2O_3$ and $SiO_2$ are good insulators used in semiconductor devices (in particular, a thin $Al_2O_3$ layer is an excellent tunneling

barrier); $SnO_2$ is a gas-sensitive material; and the transparent conductor $In_2O_3$ has been commonly used in commercial electroluminescent displays. However, as can be seen in Table 2, due to the non-radiative energy transfer to the dielectric interfaces, all the materials, except alumina and silica, quench fluorescence, and most of them quench the fluorescence to below 1% of its normal fluorescent intensity. It should be noted that: (i) the materials with the small imaginary part ($\varepsilon_{22}$) of the dielectric constants have the higher apparent quantum yields, for example, the $\varepsilon_{22}$ value for both alumina and silica is 0, and for $In_2O_3$ is very small (0.124); (ii) as seen in Table 2 and Fig. 4, at a distance of 20 Å, the calculated and experimental apparent quantum yields of Ag and $In_2O_3$ is of the order of $10^{-3}$, and the calculated and experimental values for $SnO_2$ are $7.2\times10^{-5}$ and $2.5\times10^{-4}$, respectively. This demonstrates that, as the dielectric constant varies, the trend is approximately the same for the calculated and experimental apparent quantum yields, although the experimental data fall less rapidly than the theoretical curves for alumina spacers of 10–50 Å. Therefore, the calculated apparent quantum yields in Table 2 can be considered as a characteristic parameter for evaluating the fluorescence quenching by dielectric surfaces of materials.

The mechanisms of non-radiative energy transfer to the dielectric interfaces, which depend on the specific dielectric media (dielectric constants) [15], are the excitation of surface currents and plasma resonances in free electrons of metals, or excitation of electron-hole pairs in semiconductors. According to the classical theory of absorption and dispersion, the motion of an electron bound to the nucleus is described by [16]:

$$m\frac{\mathrm{d}^2\vec{r}}{\mathrm{d}t^2}+m\Gamma\frac{\mathrm{d}\vec{r}}{\mathrm{d}t}+m\omega_0^2\vec{r}=-e\vec{E}_{\mathrm{loc}} \tag{21}$$

where $m$ is electron mass and $e$ is electron charge; $\vec{E}_{\mathrm{loc}}$ is the local electric field acting on the electron as a driving force; the term $m\Gamma(\mathrm{d}\vec{r}/\mathrm{d}t)$ represents viscous damping and provides for an energy loss mechanism; and the term $m\omega_0^2\vec{r}$ is a Hooke's law restoring force. The local field can be taken to vary in time as $e^{-i\omega t}$, so that the complex dielectric function ($\varepsilon_2=\varepsilon_{21}+i\varepsilon_{22}$) can be obtained as:

Table 2
The calculated apparent quantum yield $q_a$ for 25 dielectric systems[a]

| Material | Emission wavelength (Å) | Complex refractive indices ($n_2+ik_2$) | Dielectric constant ($\varepsilon_{21}+i\varepsilon_{22}$) | Apparent quantum yield $q_a$ (%) |
|---|---|---|---|---|
| Alumina ($Al_2O_3$) | 5890 | $1.76+i0.00$ [12] | $3.10+i0.00$ [12] | 37.7 |
| Aluminum (Al) | 5780 | $0.93+i6.33$ [14] | $-39.20+i11.8$ [14] | 0.131 |
| Barium (Ba) | 5780 | $0.88+i1.52$ [14] | $-1.54+i2.68$ [14] | 0.00494 |
| Bismuth (Bi) | 6200 | $2.24+i3.10$ [14] | $-4.60+i13.90$ [14] | 0.0102 |
| Carbon (C) | 6200 | $1.88+i0.74$ [13] | $-2.99+i2.78$ [13] | 0.0143 |
| Cesium (Cs) | 5780 | $0.264+i1.12$ [14] | $-1.19+i0.591$ [14] | 0.0122 |
| Chromium (Cr) | 6300 | $3.19+i2.26$ [14] | $5.07+i14.4$ [14] | 0.0116 |
| Copper (Cu) | 6000 | $0.186+i2.98$ [14] | $-8.85+i1.11$ [14] | 0.0418 |
| Germanium (Ge) | 5780 | $3.42+i1.35$ [14] | $9.87+i9.23$ [14] | 0.0210 |
| Gold (Au) | 6000 | $0.200+i2.90$ [14] | $-8.37+i1.16$ [14] | 0.0345 |
| Indium oxide ($In_2O_3$) | 6328 | $2.30+i0.027$ | $5.29+i0.124$ | 0.419 |
| Iridium (Ir) | 5790 | $2.13+i4.87$ [14] | $-19.2+i20.8$ [14] | 0.0306 |
| Magnesium (Mg) | 5780 | $0.480+i3.71$ [14] | $-13.5+i3.56$ [14] | 0.0412 |
| Manganese (Mn) | 5890 | $2.26+i3.71$ [14] | $-8.66+i16.8$ [14] | 0.0158 |
| Nickel (Ni) | 5890 | $1.79+i3.33$ [14] | $-7.89+i11.9$ [14] | 0.0126 |
| Platinum (Pt) | 5890 | $2.06+i4.26$ [14] | $-13.9+i17.6$ [14] | 0.0212 |
| Potassium (K) | 5780 | $0.0940+i1.57$ [14] | $-2.46+i0.295$ [14] | 0.00199 |
| Selenium (Se) | 6000 | $2.92+i0.0610$ [14] | $8.52+i0.356$ [14] | 0.275 |
| Silica ($SiO_2$) | 6000 | $1.46+i0.00$ [12] | $2.13+i0.00$ [12] | 73.6 |
| Silicon (Si) | 5890 | $4.18+i0.376$ [14] | $17.3+i3.14$ [14] | 0.0898 |
| Silver (Ag) | 6328 | $0.0295+i3.92$ | $-15.37+i0.231$ | 0.644 |
| Sodium (Na) | 5780 | $0.0270+i2.56$ [14] | $6.55+i0.138$ [14] | 0.154 |
| Tin(IV) oxide ($SnO_2$) | 6328 | $2.14+i1.97$ | $0.699+i8.43$ | 0.00717 |
| Titanium (Ti) | 5780 | $2.64+i3.42$ [14] | $-4.73+i18.3$ [14] | 0.0155 |
| Tungsten (W) | 5790 | $2.76+i2.71$ [14] | $0.274+i15.0$ [14] | 0.0130 |

[a] Emitting centers (dipoles) are located in the alumina ($\varepsilon_1=2.89+i0$) at the distance of 20 Å to the surface of dielectric media ($\varepsilon_2=\varepsilon_{21}+i\varepsilon_{22}$). The quantum yield of the free emitting state $q$ is taken to be 1. The complex refractive indices of Ag, $SnO_2$ and $In_2O_3$ were taken from Table 1, and those of the others were taken from the numbered references. Note that the experimental apparent quantum yield $q_a$ for $Al_2O_3$, Ag, $SnO_2$, and $In_2O_3$ were shown in Fig. 3, Fig. 4a,b,c, respectively (see text for detail).

$$\varepsilon_{21} = n_2^2 - k_2^2 = 1 + \frac{4\pi Ne^2}{m} \frac{(\omega_0^2 - \omega^2)}{(\omega_0^2 - \omega^2)^2 + \Gamma^2\omega^2} \quad (22)$$

$$\varepsilon_{22} = 2n_2k_2 = \frac{4\pi Ne^2}{m} \frac{\Gamma\omega}{(\omega_0^2 - \omega^2)^2 + \Gamma^2\omega^2} \quad (23)$$

where $N$ is the number of atoms per unit volume, $n_2$ and $k_2$ are the real and imaginary part of the complex refractive constant, respectively. As can be seen in Eq. (23), $\varepsilon_{22} = 0$ implies that $\Gamma = 0$, and that there is no non-radiative energy loss and only the reflection coefficient of the interface can affect the apparent quantum yields. This is why alumina and silica have high apparent quantum yields.

Fig. 5, which is given for a better understanding of the calculated quantum yields in Table 2, shows a three-dimensional representation of the calculated apparent quantum yield $q_a$ versus the real and imaginary part of the dielectric constant ($\varepsilon_2 = \varepsilon_{21} + i\varepsilon_{22}$) for emitting centers (emission wavelength 6120 Å) located in a semi-infinite non-absorbing alumina($\varepsilon_1 = \varepsilon_{11} + i\varepsilon_{12} = 2.89 + i0$) at a distance of 20 Å from the dielectric substrate ($\varepsilon_2 = \varepsilon_{21} + i\varepsilon_{22}$). For $\varepsilon_{22} = 0$ and $\varepsilon_{21} \leq 0$, the apparent quantum yield $q_a$ is equal to 1, because there is no non-radiative energy transfer and the absolute values of the reflection coefficients ($R^{\parallel}$ and $R^{\perp}$) are equal to 1 (see Eqs. (1), (3), (7) and (8)). However, for $\varepsilon_{22} = 0$ and $\varepsilon_{21} > 0$, $q_a$ is less than 1, because the absolute values of the reflection coefficients ($R^{\parallel}$ and $R^{\perp}$) are less than 1. This means there is photon absorption at the interface. As $\varepsilon_{22} > 1$, $q_a$ decreases with increasing $\varepsilon_{22}$, but there is a dip at $\varepsilon_{21} = -2.89$, because the non-radiative energy transfer, which is given by the second integral in the interval $1 \to \infty$ in Eqs. (2) and (7), has a maximum at $\varepsilon_{11} + \varepsilon_{21} = 0$, where $\varepsilon_{11}$ is the real part of the dielectric constant for alumina. Thus, fluorescence quenching due to the non-radiative energy transfer to a dielectric interface occurs only if the imaginary part of its dielectric constants is not equal to 0. On the other hand, if the imaginary part of its dielectric constants is equal to 0, fluorescence quenching is due to the radiation field energy (i.e. the far field energy) of the emitting dipole at the interface, and is determined only by the reflection coefficients of the interface.

## 5. Summary

In this work, on the basis of the classical energy flux method and energy conservation, the theoretical model for the intensity of many fluorescing molecules near the dielectric interfaces was established, and a measurable quantity, the apparent quantum yield $q_a$, describing the non-radiative energy transfer of fluorescing molecules to the dielectric interfaces, was derived. A comparison of the theory with the experiments shows that the results for metal, semiconductor and insulator interfaces can be understood within the framework of classical electromagnetic theory. Due to the non-radiative energy transfer to the dielectric interfaces at short distances, the fluorescent intensity decreases rapidly with decreasing distance, and fluorescent quenching is very strong for almost all materials — even for the transparent conductor $In_2O_3$ films, which have been commonly used in commercial electroluminescent displays. The apparent quantum yields of 25 dielectric systems have been calculated. All of the materials, except alumina and silica, quench the fluorescence, and most of them quench it to below 1% of its normal value. Thus, the apparent quantum yield $q_a$ calculated in this work may be considered as a characteristic parameter for evaluating materials for possible inclusion in diverse light-emitting devices, for example luminescent diodes and light tunnel junctions.

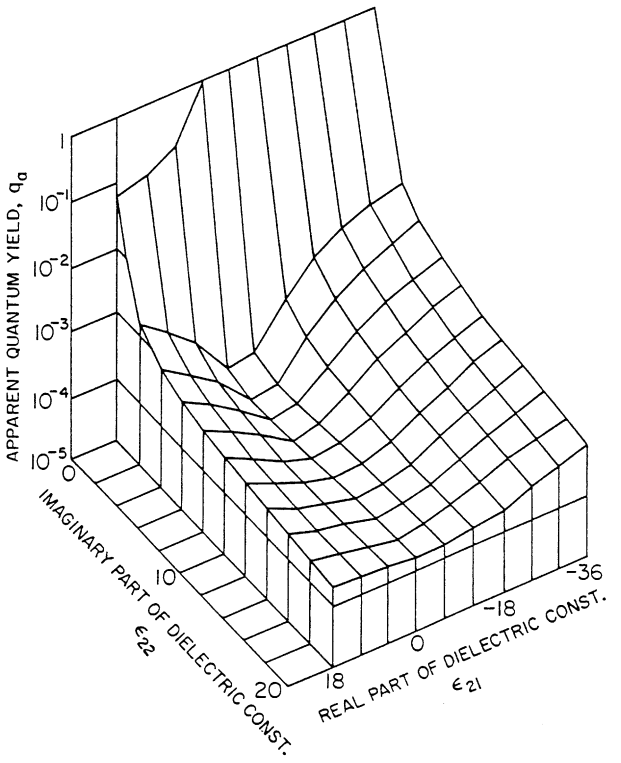


Fig. 5. The three-dimensional representation of the calculated apparent quantum yield $q_a$ for emitting centers (dipoles) located in a semi-infinite alumina ($\varepsilon_1 = 2.89 + i0$) at a distance of 20 Å from surfaces of various dielectric substrates ($\varepsilon_2 = \varepsilon_{21} + i\varepsilon_{22}$) versus the real and imaginary parts of the dielectric constants. The emission wavelength is 6120 Å and the quantum yield of the free emitting state ($q$) is taken to be 0.70.

## References

[1] V.M. Agranovich, M.D. Galanin, Electron Excitation Energy Transfer in Condensed Matter, North-Holland, Amsterdam, 1982.

[2] P. Wu, L. Brandt, Anal. Biochem. 218 (1994) 1.
[3] P.M. Whitmore, A.P. Alivisators, C.B. Harris, Phys. Rev. Lett. 50 (1982) 1092.
[4] G.T. Shubeita, S.K. Sekatskii, M. Chergui, G. Dietler, Appl. Phys. Lett. 74 (1999) 3453.
[5] D.C. Saha, D. Bhattacharjee, T.N. Misra, Opt. Mater. 10 (1998) 285.
[6] R.R. Chance, A. Prock, R. Silbey, Molecular fluorescence and energy transfer near interfaces, in: Advances in Chemical Physics XXXVII, John Wiley and Sons, New York, 1975, p. 1.
[7] M.J. Stephen, J. Chem. Phys. 40 (1964) 669.
[8] Q.Q. Shu, P.K. Hansma, P. Das, H. Metiu, J. Lumin. 40/41 (1988) 745.
[9] Q.Q. Shu, P.K. Hansma, Chin. J. Lumin. 18 (1997) 33.
[10] H. Metiu, P. Das, Annu. Rev. Phys. Chem. 35 (1984) 507.
[11] D.A. Weitz, S. Garoff, C.D. Hanson, T.J. Gramila, J.I. Gersten, Opt. Lett. 7 (1982) 89.
[12] A.J. Moses, Optical Materials Properties, IFI/Plenum Data Co, New York, 1971, pp. 4, 68.
[13] H.-H. Hagemann, W. Gudat, C. Kunz, Optical Constants from the Far Infrared to the X-Ray Region: Mg, Al, Cu, Ag, Au, Bi, C and $Al_2O_3$, Deutsches Electronen-Synchrotron DESY, 2 Hamburg 52, West Germany, 1974, Table 8, p. 1.
[14] G. Hass, L. Hadley, Optical properties of metals, in: D.E. Gray (Ed.), American Institute of Physics Handbook, McGraw-Hill, New York, 1963, p. 6.
[15] S.K. Sekatskii, G. Dietler, J. Micros. 194 (1999) 255.
[16] F. Wooten, Optical Properties of Solids, Academic Press, New York, 1972, p. 42.